nzsee
NEW ZEALAND SOCIETY FOR EARTHQUAKE ENGINEERING

FEM Analysis of Reinforced Concrete Exterior Beam-Column Joint Structures Subjected to High Varying Axial Forces

N. Zhao, Y. Suzuki & Y. Taniguchi
Osaka Metropolitan University, Osaka, Japan.

A. V. Shegay
University of Auckland, Auckland, New Zealand

M. Maeda
Tohoku University, Sendai, Japan.

ABSTRACT

Large variation of axial forces in columns in the lower stories of a high-rise reinforced concrete buildings during a severe earthquake can cause significant changes in the column-to-beam strength ratio in the exterior beam-column joints. When a column is subjected to high tensile axial forces, the column-to-beam strength ratio becomes small, leading to joint yielding and concrete damage in the joint panel zone. It has been reported that if this damage become significant, axial failure may occur in the joints when it is subjected to high compressive axial forces upon load reversal. It is important to understand this mechanism of the axial failure because it can lead to building collapse. Maeda et al. conducted experiments on exterior beam-column joints subjected to high fluctuations in axial force. They proposed a compressive strut strength equation in the joint panel after joint yielding has occurred. In this model, it is assumed that joint axial failure occurs when the compressive axial force acting on the concrete strut in the joint exceeds the estimated strut strength. However, it is concluded that further study is needed to understand the mechanism of this failure mode. To investigate the axial failure phenomenon, a 3D nonlinear FEM analysis is undertaken, referring to a previous experimental study on exterior beam-column joint specimens subjected to high varying axial forces. The results demonstrate that the analytical model closely reproduced the experimental load-deformation relationships, failure modes. It showed the ability of the model to simulate the experimental outcomes.

1 INTRODUCTION

Shiohara (2008) recently demonstrated the maximum strength of beam-column joints in reinforced concrete (RC) frame structures, designed according to the Japanese seismic design standards of (AIJ,1999) to ensure a beam yielding (total collapse) mechanism, may not achieve the anticipated design strength. It was further observed that under such conditions, joint panels can potentially fail if the column-to-beam bending strength ratio in the frame structure drops below 2.0. This failure mode is known as 'joint yielding'.

The Japanese seismic design standard (AIJ, 2021) uses a beam-column joint strength reduction factor, β_j, to account for the strength reduction observed when the beam-column joint is expected to yield. This specification serves as a basis for calculating the lateral load-carrying capacity of RC structures. When the strength reduction factor β_j exceeds 1.0, it signifies that joint yielding is effectively restrained, and the full bending moment capacity of the beam can be achieved.

During severe earthquakes, columns in the lower stories of high-rise RC buildings subjected to large variable axial forces exhibit a significant change in the column-to-beam bending ratio at the exterior beam-column joints. In the loading direction where the column experiences high tensile axial forces, the column-to-beam strength ratio decreases ($\beta_j < 1$). This leads to joint yielding and an increase in concrete damage within the joint panel. Consequently, axial failure may occur in the reverse loading direction when high compressive axial forces are induced in the previously damaged joint. This has been previously demonstrated by (Nishida et al., 2019) and shown in Figure 1.

To clarify the axial failure mechanism in beam-column joints, this study will conduct a three-dimensional nonlinear finite element method (FEM) analysis. The FEM model is based on a previous experimental study involving exterior beam-column joint specimens subjected to high varying axial forces. The validity of the FEM model will be examined through a comparison of experimental and analytical results.

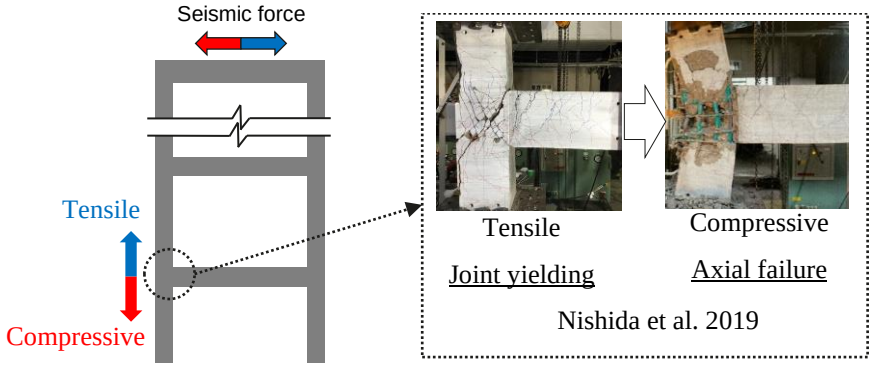

Figure 1. History of axial failure

2 ANALYSIS OVERVIEW

Three-dimensional nonlinear FEM analysis was conducted using the general-purpose code of Diana10.5 (DIANA FEA BV, 2021). In the following sections, details regarding the analysis model and the constitutive laws of the materials are provided.

2.1 Analysis Model Overview

The analytical model of this study was constructed based on the external beam-column joint specimens tested by Hagiwara et al. (2022) that were previously subjected to significant varying axial forces. Table 1 presents the specifications of the five analyzed test specimens, including dimensions, reinforcement details, strengths of reinforcing bars, and the results of material tests. All the exterior beam-column joint specimens

were designed intended for a beam yielding collapse mechanism, ensuring a joint shear margin exceeded 1.0 in accordance with the design guidelines of the AIJ standard (AIJ, 1999). The key test parameters were: (1)

Table 1. Details of the analyzed specimens

Analysis specimen		Type of specimen	T12-30 T4C5-N-13	T12-40 T4C5-N-13	T12-50 T4C5-N-13	T12-30 T4C3-N-13	T12-30 T2C3-N-13
		Failure mode of experiment	Axial failure	Beam yielding		Joint yielding	
H×L			1350×1850(mm)				
Column	Cross section		250×250(mm)				
	Main reinforcement	Bar arrangement	12-D13 (SD345)				8-D13 (SD345)
		Yield strength	406.2 (MPa)	382.3 (MPa)			
		Young's modulus	186 (GPa)	184 (GPa)			
	Hoop reinforcement	Bar arrangement	2-D6 @50 (SD295)				
		Yield strength	355.8 (MPa)	327 (MPa)			
		Young's modulus	208 (GPa)	184 (GPa)			
Beam	Cross section		225×275(mm)				
	Main reinforcement	Bar arrangement	4-D13 (SD490)				
		Yield strength	537.7 (MPa)	536.2 (MPa)			
		Young's modulus	198 (GPa)	188 (GPa)			
	Stirrup reinforcement	Bar arrangement	3-D6 @50 (SD295)	3-D6 @50 (SD295)			
		Yield strength	355.8 (MPa)	327 (MPa)			
		Young's modulus	208 (GPa)	184 (GPa)			
Joint panel	Hoop reinforcement	Bar arrangement	2-D6 3set (SD295)	2-D6 5set (SD295)	4-D6 3set (SD295)	2-D6 3set (SD295)	
		Yield strength	355.8 (MPa)	327 (MPa)			
		Young's modulus	208 (GPa)	184 (GPa)			
Properties of concrete		Compressive strength	35.1 (MPa)	35.4 (MPa)	38.9 (MPa)	40.8 (MPa)	38.3 (MPa)
		Young's modulus	32.1 (GPa)	27.8 (GPa)	28.7 (GPa)	29.1 (GPa)	27.9 (GPa)
Beam-column bending strength ratio at		(+) Loading	3.03	3.16	3.33	3.5	2.99
		(-) Loading	1.2	1.28	1.29	1.3	1.21
Main parameters							
Joint reinforcement ratio (%)			25	38	46	23	
Axial force ratio at		(+) Loading	0.5	0.5	0.5	0.31	
		(-) Loading	-0.45	-0.38			-0.14
Strength reduction rate β_j		(+) Loading	1.2	1.28	1.24	1.24	1.15
		(-) Loading	0.83	0.92	0.98	0.84	0.83

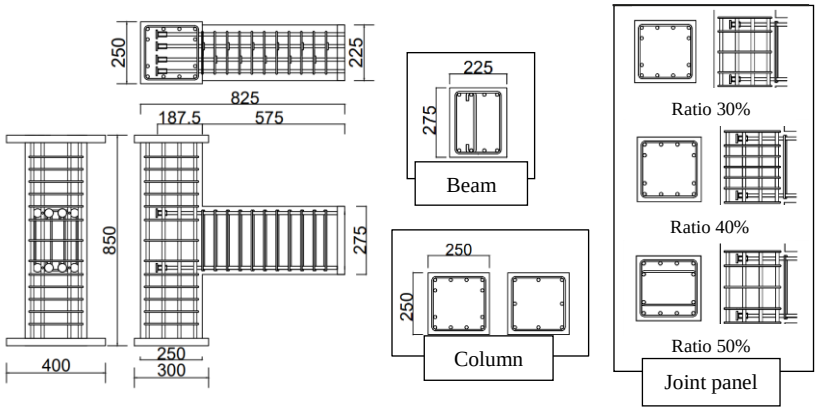

Figure 2. Details of bar arrangement

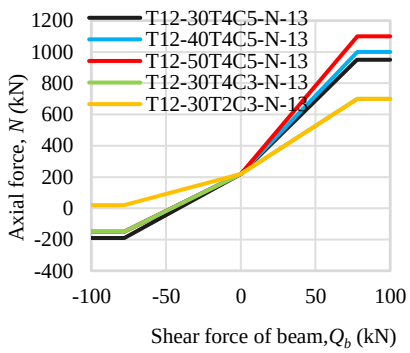

Figure 3. Varying axial force relationship with beam shear force

the joint reinforcement ratio, (2) the axial force ratio, and (3) the strength reduction factor, β_j. Figure 2 illustrates the detailed reinforcement arrangement of the test specimens. To simulate real-world conditions, varying axial loads were applied proportionally to the beam shear forces according to the relationship shown in Figure 3. The inflection point of beams and columns were assumed to be at the mid-span and mid-height of the full span, respectively. Consequently, the ends of columns and beams of each specimen were supported by pin and pin-roller connections, as illustrated in Figure 4.

2.2 Geometric Model and Boundary Conditions

The element discretization and boundary conditions of the analysis model employed in this study are illustrated in Figure 5. The concrete was represented by hexahedral solid elements, with the element size around the joint regions set at 25 × 27.5 mm. In the out-of-plane direction, the implemented element size was 25 mm. In columns, the element size of the difference between the column width and beam width was 12.5mm. The reinforcing bars were modelled as linear elements, with the support sections defined as rigid bodies. For the boundary conditions, a pin support was applied at the central nodes of the column bases; vertically movable pin roller support was provided at the central nodes of the column heads, and horizontally movable pin roller support was applied at the central nodes of the beam ends.

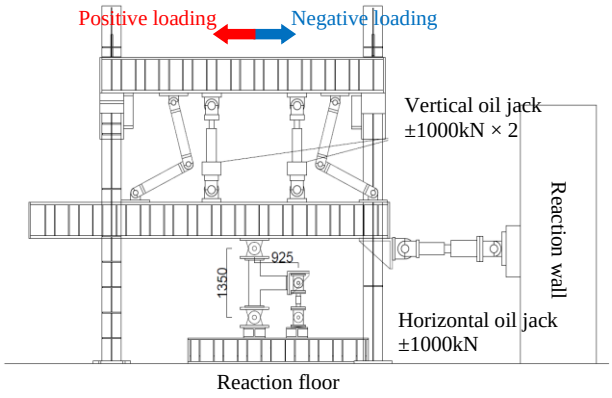

Figure 4. View of the loading setup

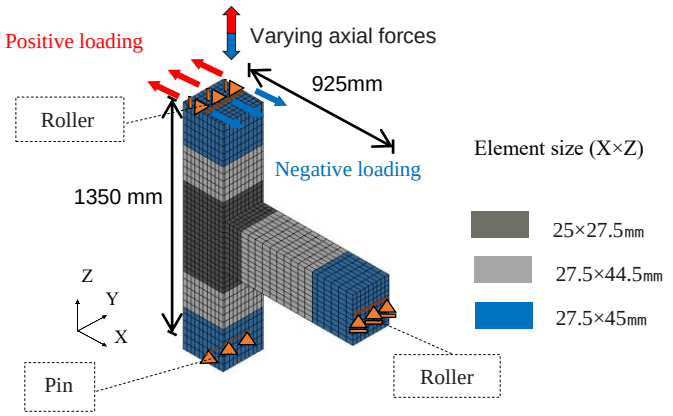

Figure 5. Element discretization and boundary conditions

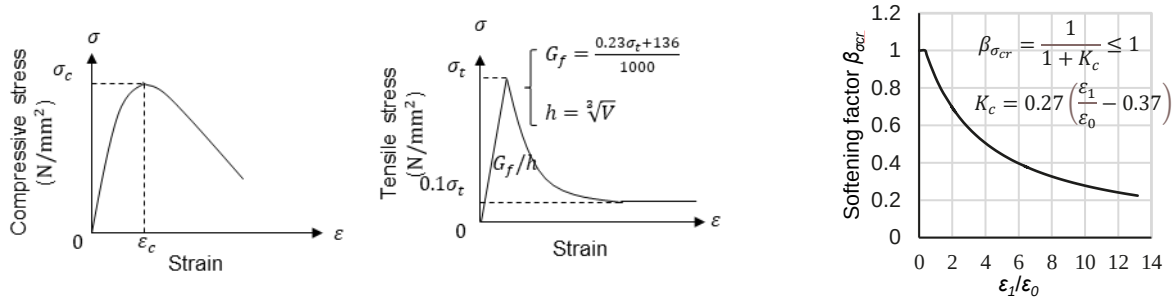

(a) Model of concrete compression behaviour.

(b) Model of concrete tension behaviour.

(c) Compressive strength reduction of concrete based on the transverse cracking model

Figure 6. Material constitutive law

2.3 Constitutive Material Laws

This section presents the constitutive laws for the concrete and reinforcement, as well as the bond-slip relationship between the reinforcement and concrete. The concrete was modeled using the rotational crack model, with the compressive constitutive law following the Concrete Standard Recommendation Model (Maekawa et al., 2003), as shown in Figure 6(a). The tensile constitutive law used the Hordijk Model (Hordijk, 1991), and the tensile fracture energy was computed using the proposed equation by Oh-oka et al. (2000). as shown in Figure 6(b). Additionally, the reduction in compressive strength due to transverse cracking in concrete (compression softening) was modelled using recommendations by Vecchio and Collins (1993), as shown in Figure 6(c). The constitutive material law for reinforcement was bilinear, with a post-yield stiffness set to 1/100 of the initial stiffness. The main reinforcement in the columns and beams were treated as bond-slip embedded reinforcement elements. The bond stress-slip relationship with concrete was modelled using the CEB-FIP Model (FIB, 2012), while the shear reinforcement was treated as a fully embedded reinforcement element.

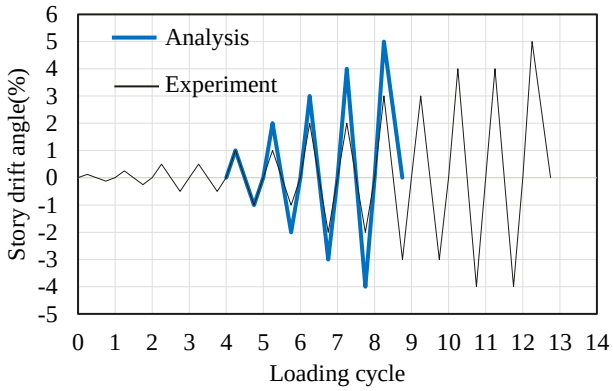

Figure 7. Loading protocol of experiment and FEM analysis

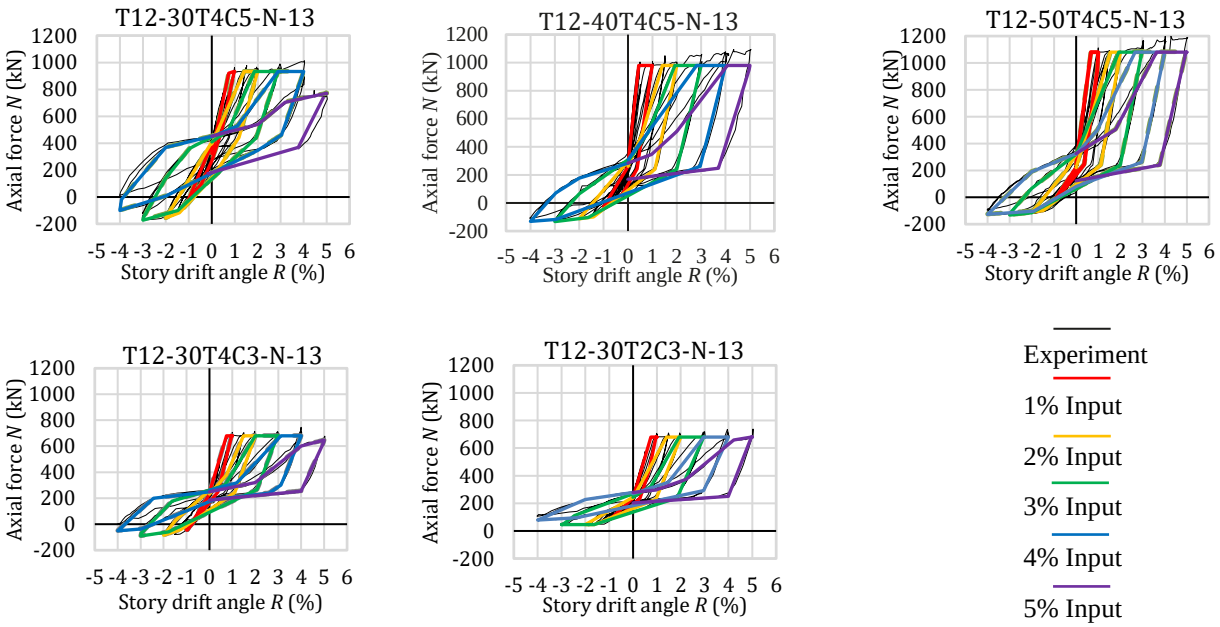

Figure 8. Axial force protocol used in FEM analysis.

2.4 Loading Method

For the loading method, a 1 mm alternating horizontal displacement was applied to the column head while concurrently subjecting it to varying axial loads in the vertical direction. Figure 7 illustrates the loading protocol employed in both the analysis and experiment. In the experiment, two cycles were conducted at story drift angles ranging from R = ±1/800 to +1/20. In the analysis, the loading protocol was similar to the experiment, with two changes to reduce computational time – firstly, the story drift angles below R = ±1/100 were omitted, and the second loading cycle was not simulated. Given the practical limitations in automatically inputting variable axial force proportionally to the beam shear force, a simplified protocol was adopted in the analysis, as shown in Figure 8. The black line in the figure depicts the relationship between the introduced axial force and the story drift angle observed in the experiment and the coloured lines show the approximation used in the analysis.

3 RESULTS AND DISCUSSION OF THE ANALYSIS

In this chapter, the results of the FEM analysis and validation against the experimental results is presented.

3.1 Relationship between the Story Shear Force and Story Drift Angle

Figure 9 presents the relationships between the story shear force and story drift angle, comparing the results of the analysis with those of the experiment. As a result, the maximum force in both positive and negative loadings in the analysis were simulated to be approximately equal to those observed in the experiment. The phenomenon of the positive-side maximum strength surpassing the negative-side maximum strength across all specimens can be attributed to the high-level varying axial forces acting on the columns, resulting in significant variations in the column-beam strength ratio. Despite the analysis demonstrating a stiffness similar to that of the experiment, the analysis exhibited narrower loops and thus a lower energy absorption capacity than the experiment.

For T12-50T4C5-N-13, both positive and negative loadings reached the theoretical shear force (dotted black line) at the ultimate flexural strength of the beam, indicating a beam bending failure mode. For other specimens, the maximum force in the negative loading was below the theoretical shear force at the ultimate

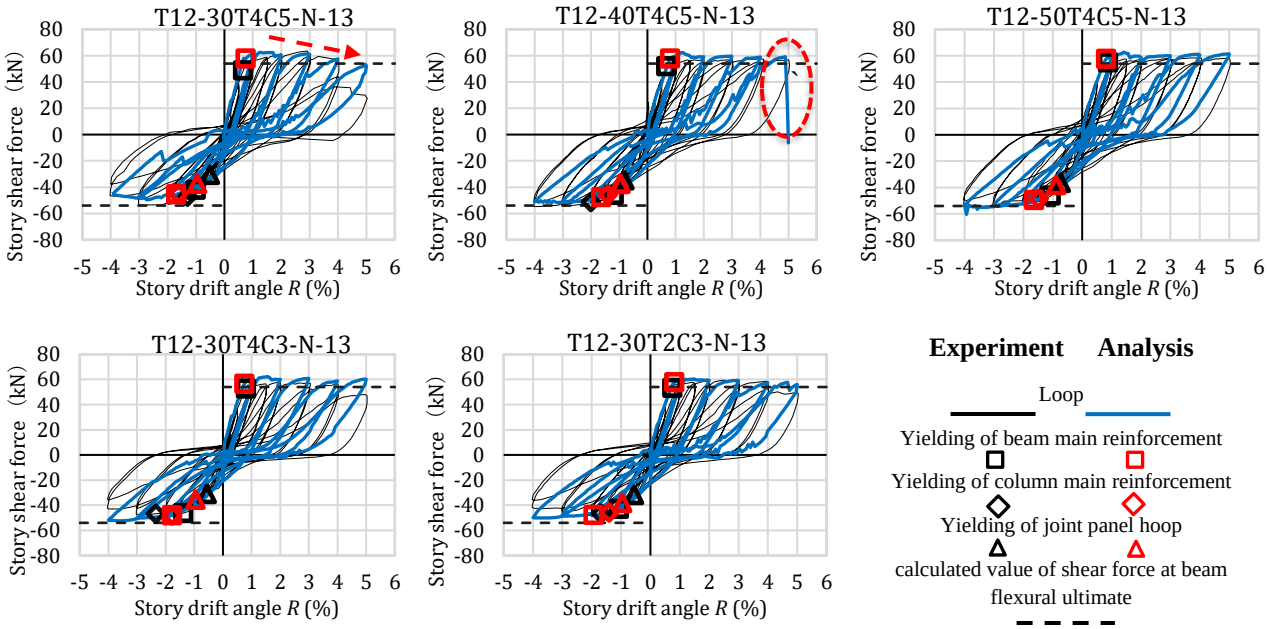

Figure 9. Story shear force and story drift angle curves

flexural strength of the beam, indicating a joint yielding failure mode. Moreover, a higher ratio of the joint reinforcement (e.g. T12-30T4C5-N-13 compared with T12-50T4C5-N-13) demonstrated to be associated with the negative-side maximum resistance approaching the resistance at the ultimate flexural strength of the beam, suggesting the potential for the lateral reinforcement of joints to suppress joint yielding failure. Additionally, for T12-30T4C5-N-13, simulated results were able to simulate the gradual strength loss in the positive direction observed in the experiment, though the rate of reduction was faster at R = +5% in the experiment because an axial failure was observed. For T12-40T4C5-N-13, the analysis did not exhibit a gradual decrease in the positive-side resistance, but rather a rapid decrease just before R = +5%, leading to axial failure. Although the ratio of the joint reinforcement of T12-40T4C5-N-13 is larger than T12-30T4C5-N-13, the rapid axial failure can be attributed to the greater compressive forces acting on T12-40T4C5-N-13 at R = +5.0% compared to T12-30T4C5-N-13, as depicted in Figure 8. Furthermore, the story drift angles at the time of rebar yielding were generally similar, with no significant differences observed.

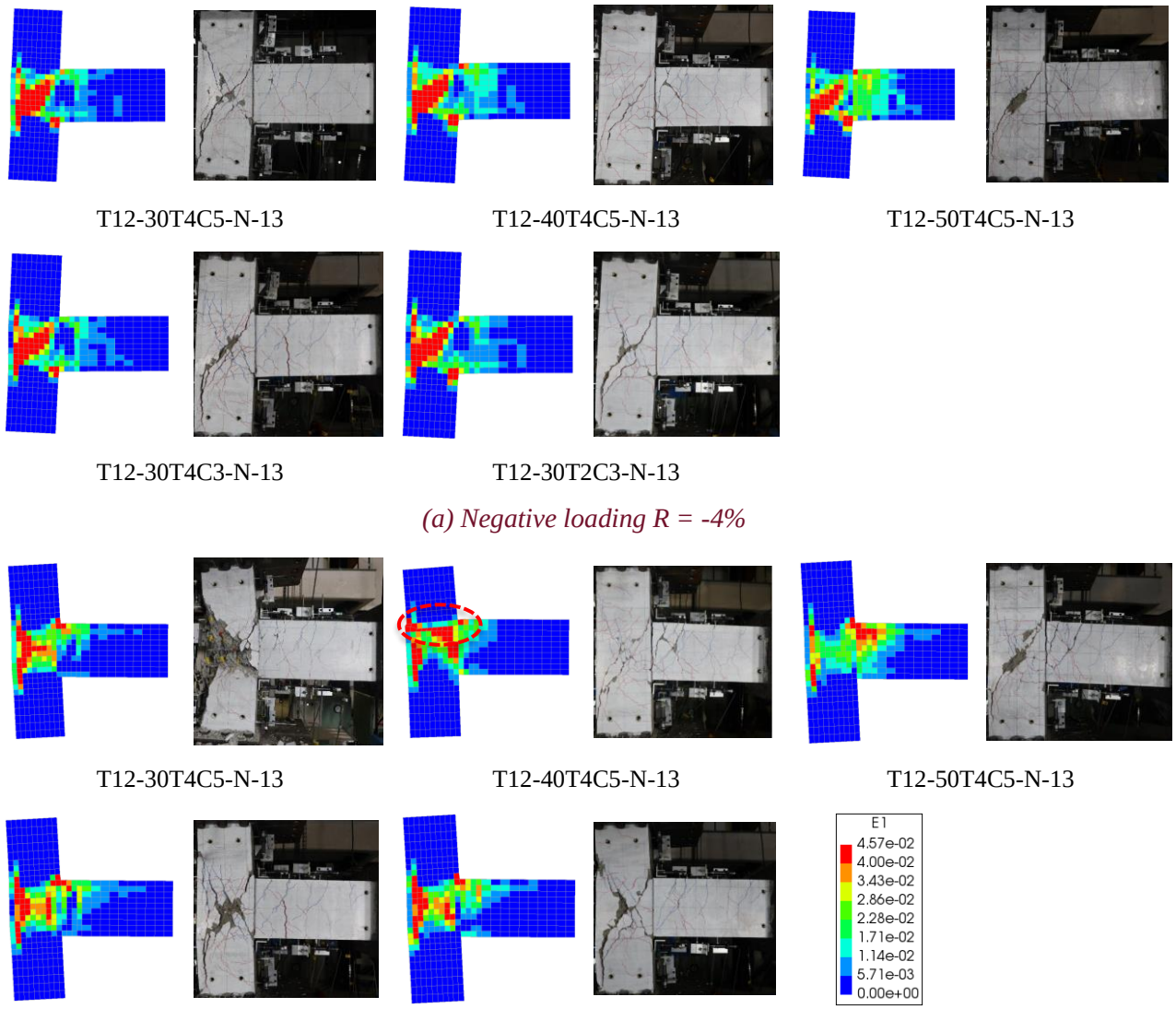

(a) Negative loading R = -4%

(b) Positive loading R = +5%

Figure 10. Comparison of the analytical and experimental failure characteristics (coloured images: analysis; black/white images: experimental)

3.2 Failure characteristics

Figure 10 presents the maximum principal strain plots at story drift angles of R = -4.0% and R = +5.0%. The red areas in the figure represent locations where the maximum principal strain exceeds 4.0% and cracks that are 1.0 mm or large have occurred. The damage pattern in the joint area was apparently concentrated in the diagonal central part at R = -4.0 %. The model of T12-50T4C5-N-13 exhibited the least damage within the joint area, which can be attributed to the increase in the transverse reinforcement quantity in the joint. Instead, the damage tended to concentrate more at the beam ends, as intended in design.

Conversely, at R = +5.0%, the influence of the compressive axial forces resulted in the damage being concentrated at the beam ends. Additionally, owing to damage occurring during loading in the negative direction (i.e., joint in tension), compressive axial forces eventually led to a state of collapse. T12-50T4C5-N-13 exhibited a lower level of damage within the joint area on the negative side compared to the other models; thus, the specimen could sustain higher compressive strength on the positive side. In the experimental results of T12-30T4C5-N-13, due to severe concrete spalling/crushing in the joint panel, and buckling of the longitudinal bars in the column, significant axial deformation occurred, ultimately resulting in axial failure. While the analysis results maintained axial deformation, the simulated condition of concrete crushing in the joint panel was believed to be consistent with the experimental results. Despite T12-40T4C5-N-13 having a greater quantity of reinforcement in the joint area compared to T12-30T4C5-N-13, the analysis results revealed a loss of the ability to maintain axial deformation, resulting in axial failure. As previously mentioned in section 3.1, this is thought to be because T12-40T4C5-N-13 was subjected to higher axial compression forces than T12-30T4C5-N-13.

4 CONCLUSION

In this paper, analysis results from FEM models of exterior beam-column joint specimens subjected to large varying axial forces, are presented. Although there are differences between the experimental and analytical results regarding the final failure modes of T12-30T4C5-N-13 and T12-40T4C5-N-13, the results are consistent in terms of maximum yield strength, the timing of yield in each reinforcing bar, stiffness, and failure properties. This comparison demonstrates that the experiment results can be effectively reproduced using the FEM modelling methodology used in this study.

5 ACKNOWLEDGEMENTS

This study was carried out as a part of the research projects of "Research Committee for Mechanical Anchorage System" (chaired by Prof. Maeda of Tohoku University) in NEWTECH Research Society. The support and cooperative works for the research are gratefully acknowledged.

6 REFERENCES

Architectural Institute of Japan (1999). "*Design Guidelines for Earthquake Resistant Reinforced Concrete Buildings Based on Inelastic Displacement Concept*". Architectural Institute of Japan, Tokyo, 245pp.

Architectural Institute of Japan (2021). "*AIJ Standard for Lateral Load-carrying Capacity Calculation of Reinforced Concrete Structures*". Architectural Institute of Japan, Tokyo, 198pp.

FIB (2012). "*CEB-FIP MODEL CODE 2010 DESIGN CODE*", the International Federation for Structural Concrete, Lausanne, 249pp. https:// doi.org/10.35789/fib.BULL.0055

DIANA FEA BV (2021). DIANA Finite Element Analysis DIANA Documentation Release 10.5.

Hagiwara H., Suzuki Y., Koike T., Maeda M. (2022). Study of the parameters influencing the axial collapse mechanism of RC exterior beam-column joint, *Japan Concrete Institute*, Vol44, No2, 469-474pp.

Hordijk D. A. (1991). Local Approach to Fatigue of Concrete, Ph.D. thesis, Delft University of Technology.

Maekawa, K., Okamura, H., and Pinanmas A. (2003). "*Nonlinear Mechanics of Reinforced Concrete*". ISBN-13: 978-0415271264, CRC Press, London. https://doi.org/10.1201/9781482288087

Nishida T., Suzuki Y., Maeda M. (2019). "Experimental study on the influence of varying axial force on the fracture properties and structural performance of an exterior beam-column joint where the joint yields". *Japan Concrete Institute*, Vol41, No2, 253-258pp. https://data.jci-net.or.jp/data_pdf/41/041-01-2043.pdf

Oh-oka T., Kitsutaka Y., Watanabe K., (2000). "Influence of short cut fiber mixing and curing time on the fracture parameters of concrete". *J. Struct. Constr. Eng., AIJ*, No529, 1-6pp.

Shiohara H. (2008). "Reinforced concrete beam-column joint: failure mechanism overlooked". *J. Struct. constr. Eng., AIJ*, Vol.73, No631, 1641-1648pp. https://doi.org/10.3130/aijs.73.1641

Vecchio F. J., Collins M. P. (1993). Compression response of cracked reinforced concrete, *J. Struct. Eng. ASCE*, Vol119, No12, 3590-3610pp. https://doi.org/10.1061/(ASCE)0733-9445(1993)119:12(3590)